Approaching extremely low thermal conductivity by crystal structure engineering in $Mg_2Al_4Si_5O_{18}$

Yiran Li
High-performance Ceramics Division, Shenyang National Laboratory for Materials Science, Institute of Metal Research, Chinese Academy of Sciences, Shenyang 110016, China; and University of Chinese Academy of Sciences, Beijing 100049, China

Jiemin Wang and Jingyang Wang[a)]
High-performance Ceramics Division, Shenyang National Laboratory for Materials Science, Institute of Metal Research, Chinese Academy of Sciences, Shenyang 110016, China

(Received 18 September 2015; accepted 20 November 2015)

One of the challenges in developing a low thermal conductivity material addresses on searching lightweight ceramic without heavy or rare-earth (RE) elements. $Mg_2Al_4Si_5O_{18}$ interests us for its very low density and complex crystal structure. The first-principle calculations were performed to predict mechanical and lattice thermal conductivity of hexagonal and orthorhombic phases of $Mg_2Al_4Si_5O_{18}$. According to Debye approximation and the Slack model, the lattice thermal conductivity varies with temperature in 804.6/T and 719.7/T, yielding 2.95 and 2.64 W/(m·K) at room temperature, respectively. The high temperature limits of thermal conductivities are as low as 1.33 and 1.29 W/(m·K). The thermal conductivities of both polymorphs of $Mg_2Al_4Si_5O_{18}$ are lower than most of RE-containing silicates and zirconates. The present work suggests that $Mg_2Al_4Si_5O_{18}$ is a promising lightweight ceramic with extremely low thermal conductivity. We also highlight that enhancing complexity of the crystal structure rather than incorporating heavy RE elements may be an alternative wisdom to explore lightweight thermal insulators.

I. INTRODUCTION

Materials with low thermal conductivity have long been investigated for their broad applications, especially as thermal insulation materials. Researchers usually follow a selection guideline proposed by D.R. Clarke[1] to search for candidate materials. It says that materials with low thermal conductivity should satisfy four principal conditions: a large molecular weight, a complex crystal structure, nondirectional bonding, and a large number of different atoms per molecule. Accordingly, many studies have been focused on candidates, such as rare-earth silicates,[2] zirconates,[3,4] and phosphates,[5,6] since introducing rare-earth elements is an effective way to increase the atomic mass as well as bonding heterogeneity. However, in view of the sustainable development and cost minimization of thermal insulators, it is imminent to explore a new strategy in which rare-earth elements are no longer crucial to reduce thermal conductivity.

As an aluminosilicate free of a rare-earth element, magnesium cordierite ($Mg_2Al_4Si_5O_{18}$) was taken as the cutting-in point to enrich the scope of material selection. It has been reported to own very low thermal conductivity at room temperature (RT) [~3 W/(m·K)][7,8] compared with other candidates (details summarized in Table I[7–10]). At the same time, the density of $Mg_2Al_4Si_5O_{18}$ is much lower (~2.51 g/cm^3) than most thermal insulation materials. Recently, some lightweight materials with low thermal conductivity like MPO_4,[5] MP_2O_7,[11,12] and $MSiO_4$[13] have attracted more attention, because of their broad applications as thermal insulators, flame resistance, and fireproofing materials in fields of transportation and construction industry. Their lattice thermal conductivities were comprehensively predicted using first-principles calculations.

Besides the low density and low thermal conductivity, $Mg_2Al_4Si_5O_{18}$ engages our attention for its specific complex crystal structure. Many studies have shown that one promising approach to reduce thermal conductivity is to introduce guest atoms into the crystalline framework, e.g., clathrate and skutterudite, since the loosely coupled guests are associated with high thermal resistivity.[14] As is shown in Fig. 1, either of the two polymorphs[15] of $Mg_2Al_4Si_5O_{18}$ provides a specific structure to host Mg atoms at the interstitial sites of the framework of [AlO_4] and [SiO_4] tetrahedra. It is expected that this characteristic structure may play a pivotal role in reducing the thermal conductivity of $Mg_2Al_4Si_5O_{18}$.

In addition, $Mg_2Al_4Si_5O_{18}$ is well-known for its ultralow coefficient of thermal expansion, good thermal shock resistance, excellent stability up to high temperatures,

Contributing Editor: Yanchun Zhou
[a)]Address all correspondence to this author.
e-mail: jywang@imr.ac.cn
DOI: 10.1557/jmr.2015.367

 © Materials Research Society 2015

https://doi.org/10.1557/jmr.2015.367 Published online by Cambridge University Press

good chemical stability, and dielectric properties.[16–23] It is usually used as refractory materials, electronic packaging materials, bio-ceramics, infrared radiation materials, filtering material for molten metals, and honeycomb catalyst carrier in automobile exhaust system. All these great properties and performance of $Mg_2Al_4Si_5O_{18}$ support it as a strong candidate for precisely evaluating the intrinsic lattice thermal conductivity.

In this work, first-principle calculations are performed to study the lattice thermal conductivity of two cordierite polymorphs, α-$Mg_2Al_4Si_5O_{18}$ and β-$Mg_2Al_4Si_5O_{18}$. The equilibrium crystal structure, Mulliken population and bonding characteristics are calculated as well. The full set of elastic constants or stiffness matrix, polycrystalline shear modulus, bulk modulus, Young's modulus, and Poisson's ratio are computed, from which sound velocities, Debye temperature and Grüneisen parameter are also derived. Anisotropic elastic stiffness, such as directional Young's modulus is discussed. Finally, temperature dependence of thermal conductivity as well as the minimum value are predicted by the Slack model[24] and Clarke model,[1] respectively. Our results demonstrate that the low thermal conductivity of $Mg_2Al_4Si_5O_{18}$ is closely related to its complex crystal structure, and that crystal structure engineering provides us an alternative opportunity to discover lightweight thermal insulators.

TABLE I. Density (g/cm^3) and thermal conductivity [W/(m·K)] at room and high temperature of candidates for low thermal conductivity applications.

Compound	Density	Thermal conductivity @RT	Thermal conductivity @1273 K
(3%mol)YSZ[8]	6.0	2.9	2.3
$La_2Zr_2O_7$ (Ref. 8)	6.05	3.2	1.56
$LaPO_4$ (Ref. 8)	5.07	3.61	1.8 (973 K)
α-$AlPO_4$ (Ref. 5)	2.72	11.7	2.75
YAG[8]	4.55	10.3	3.0
Y_2SiO_5 (Ref. 9)	4.09	1.86	1.31
γ-$Y_2Si_2O_7$ (Ref. 10)	4.48	4.91	1.95
Mullite[8]	3.27	5.4	3.3 (1400 K)
ZrO_2 (Ref. 8)	5.85	8.2	2.17
$LaMgAl_{11}O_{19}$ (Ref. 8)	4.26	3.2	2.7
$BaZrO_3$ (Ref. 8)	6.23	...	3.42
$Mg_2Al_4Si_5O_{18}$ (Ref. 7)	2.52	2.5	...

II. CALCULATION METHODS

A. Computational details

The theoretical calculations were performed using first principles based on density functional theory[25] as implemented in the CASTEP code.[26] Vanderbilt-type ultrasoft pseudo potentials (US-PP)[27] and a plane-wave expansion of the wave functions were used. The local density approximation[25] was selected to describe the exchange correlation functional. The energy cutoff was fixed to be 450 eV. The *k*-point sampling of the Brillouin zone was constructed by using the Monkhorst–Pack method[28] with 2 × 2 × 2 grids in primitive cells. All atomic positions and lattice parameters were fully relaxed using Broyden–Fletcher–Goldfarb–Shanno[29] minimization scheme until the difference on total energy is within 5.0×10^{-6} eV/atom, maximum

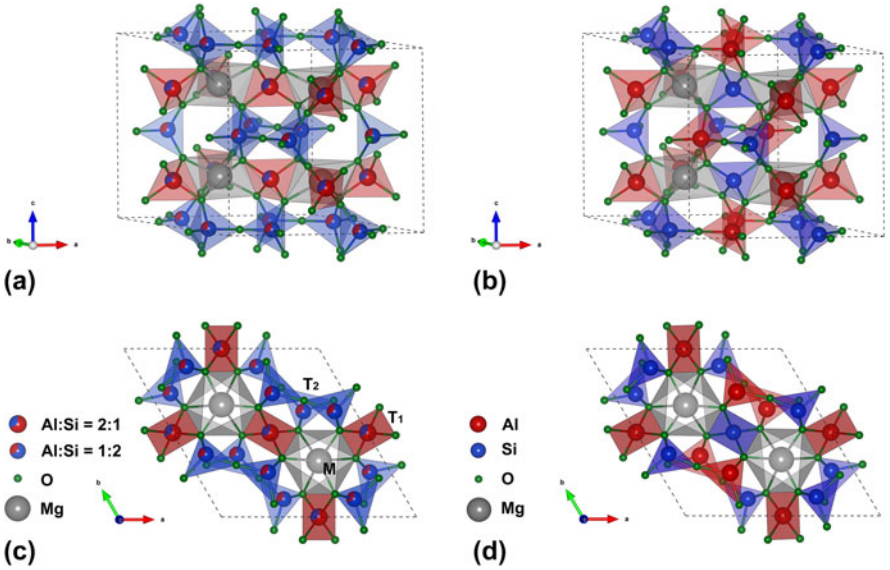


FIG. 1. Crystal structures of (a) α-$Mg_2Al_4Si_5O_{18}$ and (b) β-$Mg_2Al_4Si_5O_{18}$, as well as (c) and (d) their projections along the *c* axis (Mg in gray, Al in red, Si in blue and O in green).

https://doi.org/10.1557/jmr.2015.367 Published online by Cambridge University Press

ionic Hellmann–Feynman force within 0.01 eV/Å, maximum stress within 0.02 GPa and maximum ionic displacement within 5×10^{-4} Å.

As color coded in Fig. 1, the T_1 tetrahedral site is disorderly occupied by Al/Si in the ratio of 2 to 1 while the T_2 site have the ratio of 1 to 2. Thus, virtual crystal approximation (VCA)[30] within the US-PP method was used to model the fractional occupancy of Al/Si atoms of α-$Mg_2Al_4Si_5O_{18}$. VCA assumes that on each potentially disordered site there is a virtual atom which interpolates between the characters of the actual components. This method is reasonably accurate to model Al/Si disorder in silicates, such as hollandite and gehlenite,[31] and it could well reproduce the crystal structure, structural stability, and bulk modulus.

After applying two strain patterns and calculating the resultant stress tensors, the second-order elastic coefficients of α- and β-$Mg_2Al_4Si_5O_{18}$ were derived by linear fitting of the stress–strain relationship, as implemented by Milman and Warren.[32] Three positive and three negative amplitudes were applied for each strain component with a maximum strain value of 0.3% to avoid the nonlinear stress–strain relationship at higher strain values. Convergence tolerance for optimization on atomic internal freedoms was selected as the difference in the total energy within 1×10^{-6} eV/atom, the ionic Hellmann–Feynman force within 0.002 eV/Å and the maximum ionic displacement within 1×10^{-4} Å. The choice of present computational parameters ensures good agreement with experimental values of the crystal structure and elastic properties.

B. Structural distortion

For an equilibrium crystal structure, definition of the degree of distortion Δ_d of the coordination polyhedron[33] yields:

$$\Delta_d = \frac{1}{n}\sum_n \left(\frac{d(M-O)_n - \langle d(M-O)_n\rangle}{\langle d(M-O)_n\rangle}\right)^2 \quad , \qquad (1)$$

where $d(\text{M–O})_n$ and $<d(\text{M–O})_n>$ are the M–O bond length for the nth O atom and the average length of M–O bonds in the polyhedron, respectively. It is expected that the higher the value of Δ_d is, the larger the degree of distortion of the polyhedron is.

C. Elastic properties

Bulk modulus B and shear modulus G for crystalline aggregates can be estimated from single-crystal elastic constants with the well-established Voigt–Reuss–Hill approximation.[34] According to the conversion formulas between elastic moduli,[35] the Young's modulus E, and Poisson's ratio ν can be calculated according to the bulk modulus B and shear modulus G:

$$E = 9BG/(3B+G) \quad , \qquad (2)$$

$$\nu = (3B-2G)/[2(3B+G)] \quad . \qquad (3)$$

D. Lattice thermal conductivity

Slack suggested the following description for lattice thermal conductivity κ [W/(m·K)] in a temperature range in which heat conduction is dominated by Umklapp scattering among acoustic phonons:[24,36]

$$\kappa = \frac{B_\gamma \bar{M}\delta\theta_D^3}{\gamma^2 N_{cell}^{2/3} T} \quad , \qquad (4)$$

where $\bar{M}$ is the average mass of atoms in g/mol, δ^3 is the average volume of atoms in m^3, θ_D is the Debye temperature in K, γ is the Grüneisen parameter, N_{cell} is the number of atoms per primitive unit cell, and B_γ is a coefficient related to γ:

$$B_\gamma = \frac{2.43 \times 10^{-8}}{1-(0.514/\gamma)+(0.228/\gamma^2)} \quad . \qquad (5)$$

Due to the significant complexity of the crystal structure and chemical bonding in $Mg_2Al_4Si_5O_{18}$, it is difficult to access the mode Grüneisen parameter[37] from the phonon dispersion. Therefore, in this work, the acoustic γ[37–40] is calculated to represent the anharmonicity of phonon scattering. The method is based on an average of lattice vibrational frequency, i.e., equalizing vibration energy of acoustic phonon to the energy of elastic wave propagation in a continuum approximation of polycrystalline. Hence, the acoustic Grüneisen parameter γ can be directly derived from Poisson's ratio ν or sound velocities as[38,41]:

$$\gamma = \frac{3}{2}\left(\frac{1+\nu}{2-3\nu}\right) = \frac{9}{2}\frac{v_l^2 - 4v_s^2/3}{v_l^2 - 2v_s^2} \quad . \qquad (6)$$

Further, we use the definition of Debye temperature[24,39] from elastic constants as follows:

$$\theta_D = \frac{h}{k_B}\left[\frac{3}{4\pi}\left(N_{cell}\frac{N_A\rho}{M_{cell}}\right)\right]^{1/3} v_m \quad , \qquad (7)$$

where h is the Planck constant in J·s, k_B is the Boltzmann constant in J/K, N_A is the Avogadro constant, ρ is density in kg/m^3, M_{cell} is the mass per primitive cell in kg, and v_m is the mean sound velocity determined by density and elastic constants[40]:

$$v_m = \left[\left(v_l^{-3} + 2v_t^{-3}\right)/3\right]^{-1/3} \quad , \qquad (8)$$

https://doi.org/10.1557/jmr.2015.367 Published online by Cambridge University Press

$$v_l = (G/\rho)^{1/2}$$
$$v_t = [(B + 4G/3)/\rho]^{1/2} \quad , \tag{9}$$

here v_l and v_s are the longitudinal and transverse sound velocity, respectively.

At a high temperature limit, lattice thermal conductivity approaches its minimum value and remains independent to temperature thereafter. Clarke[1] assumed that the minimum phonon mean free path converges to the average interatomic distance in the material at high temperature and approximated different atoms in a molecule with an equivalent atom having a mean atomic mass of M_{cell}/n_{cell}. Therefore, the theoretical minimum thermal conductivity can be calculated by:

$$\kappa \rightarrow k_B v l \rightarrow k_B v l_{min} \rightarrow \kappa_{min}^{Clarke} \rightarrow k_B v_m \left(\frac{M_{cell}}{N_{cell}\rho N_A}\right)^{-2/3} . \tag{10}$$

III. RESULTS AND DISCUSSION

A. Crystal structure and chemical bonding

Cordierite mainly exists in two thermodynamically stable polymorphs, including an Al/Si disordered hexagonal phase α-$Mg_2Al_4Si_5O_{18}$ (*P*6/mcc, Z = 2) and an Al/Si ordered orthorhombic phase β-$Mg_2Al_4Si_5O_{18}$ (*Cccm*, *Z* = 4).[15,42,43] Figure 1(a) is the crystal structure of α-$Mg_2Al_4Si_5O_{18}$ and Fig. 1(c) is its projection along the *c* axis. Al and Si atoms are illustrated in red and blue so that the Al/Si disordered sites are represented as two-colored spheres with a fixed red/blue ratio. Figs. 1(b) and 1(d) are the crystal structure and *c*-axis projection, respectively, of β-$Mg_2Al_4Si_5O_{18}$. It is clear that both crystal structures essentially consist of the framework of [AlO_4] and [SiO_4] tetrahedra with [MgO_6] octahedral coordination. To be specific, the [AlO_4] and [SiO_4] tetrahedra can be divided into two types: corner-sharing T_2 tetrahedra forming a distorted hexagonal ring which is contra rotated by ~30° in the adjacent T_2 ring layer; and T_1 tetrahedra connecting neighboring T_2 rings as well as sharing two opposite edges with octahedra that coordinate Mg atoms. The Mg atoms are located in the distorted octahedra that share edges with three T_1 tetrahedra. The main difference between α- and β-$Mg_2Al_4Si_5O_{18}$ is whether there exists Al/Si ordering. Specifically speaking, in the high-temperature phase α-$Mg_2Al_4Si_5O_{18}$ that is stable above 1450 °C, the Al and Si atoms are distributed over two sets of tetrahedral sites: three T_1 and six T_2 sites per formula unit. The Al and Si distribution involves: two Al and one Si disorderly occupying the T_1 tetrahedra; and two Al and four Si disorderly present on the T_2 tetrahedra. In the low-temperature phase β-$Mg_2Al_4Si_5O_{18}$ that is stable under 1450 °C, the tetrahedra at T_1 sites are grouped into two non-equivalent types: $T_1$1 and $T_1$6, while the tetrahedra at T_2 sites are denoted into three non-equivalent types: $T_2$1, $T_2$3, and $T_2$6. The third symbol of each label represents the symmetry operation (1 for identity map, 3 for the third-turn, and 6 for the sixth-turn) that correlates the atoms in equivalent sets. Within this new structure, Al and Si atoms are able to form a completely ordered distribution[43] (see details in Table II).

The optimized lattice parameters of α- and β-$Mg_2Al_4Si_5O_{18}$ are compared with the experimental data[15] in Table III. Based on the results, the deviations of theoretical lattice parameters from the experimental values for α-$Mg_2Al_4Si_5O_{18}$ are 1.08% for *a* and *b*, and 1.54% for *c*; and the deviations for β-$Mg_2Al_4Si_5O_{18}$ are 0.90% for *a* and *b*, and 1.10% for *c*.

Table IV lists the degrees of distortion Δ_d of coordination polyhedra for α- and β-$Mg_2Al_4Si_5O_{18}$. It is observed that the bond lengths of T_1 ($T_1$1 and $T_1$6) sites are slightly larger than those of T_2 ($T_2$1, $T_2$3 and $T_2$6) sites. Besides, Si–O bonds are shorter than Al–O bonds, which are normally identified in aluminosilicates. Interestingly, the bond lengths at both T_1 and T_2 sites in α-$Mg_2Al_4Si_5O_{18}$ are slightly smaller than their counterparts ($T_1$1, $T_1$6 and $T_2$1, $T_2$3, and $T_2$6) in β-$Mg_2Al_4Si_5O_{18}$. Accordingly, the degree of distortions for all three kinds of polyhedra in α-$Mg_2Al_4Si_5O_{18}$ is smaller than those in β-$Mg_2Al_4Si_5O_{18}$. When modeling the Al/Si disorder in α-$Mg_2Al_4Si_5O_{18}$, the VCA method eliminates the difference between Si–O and Al–O bonds by the virtually averaged $Si_{1/3}Al_{2/3}$–O and $Si_{2/3}Al_{1/3}$–O bonds. Therefore, it neglects such effects as local distortions around atoms in α-$Mg_2Al_4Si_5O_{18}$. Furthermore, distortions of T_1 ($T_1$1 and $T_1$6) and M polyhedra are almost zero while the degrees of distortion of tetrahedra at T_2 ($T_2$1, $T_2$3 and $T_2$6) sites are higher than those at T_1 ($T_1$1 and $T_1$6) and M sites. Combined with the research studies on structure dependence on temperature or pressure,[20,44,45] the conclusion is easily drawn that T_1 ($T_1$1 and $T_1$6) tetrahedra and M octahedra play more active roles than T_2 ($T_2$1, $T_2$3 and $T_2$6) tetrahedra in responding to deformation. It is supposed that since T_1 ($T_1$1 and $T_1$6) tetrahedra are less constrained by the symmetry compared to T_2 ($T_2$1, $T_2$3 and $T_2$6) tetrahedra, they can accommodate distortion by rotating or bending about adjoining tetrahedrons. This mechanism results in

TABLE II. Tetrahedral sites in the $Mg_2Al_4Si_5O_{18}$ polymorphs.

Hexagonal form	Orthorhombic form	Site content
3 T_1 sites	2 $T_1$1 sites	2 Al
	1 $T_1$6 site	1 Si
6 T_2 sites	2 $T_2$1 sites	2 Si
	2 $T_2$3 sites	2 Si
	2 $T_2$6 sites	2 Al

https://doi.org/10.1557/jmr.2015.367 Published online by Cambridge University Press

near-zero distortion in T_1 ($T_1$1 and $T_1$6) tetrahedra. On the contrary, T_2 ($T_2$1, $T_2$3 and $T_2$6) tetrahedra restricted by the six-member rings are less free for response to strain. Therefore, the degrees of distortions of T_2 ($T_2$1, $T_2$3 and $T_2$6) and M sites are much larger than those for T_1 ($T_1$1 and $T_1$6) sites. And it is also noted that T_1 ($T_1$1 and $T_1$6) and M sites are closely related to the interstitial Mg atoms. Therefore, the weakly bound Mg atoms, which can be regarded as the guest atoms within the framework of Al and Si tetrahedra, may reduce thermal conductivity by effectively scattering phonons. In addition, the distortion of Si tetrahedra is smaller than that of Al tetrahedra since Si–O bonds are stiffer than Al–O bonds. Mulliken population[46] of Si–O and Al–O bonds in β-$Mg_2Al_4Si_5O_{18}$ is analyzed in Fig. 2 to support this explanation. The population of Si–O bond is larger than that of Al–O bond, indicating Si–O bond is stronger than the latter one. The Mulliken population of ionic M–O bond is negative and is not shown here.

B. Elastic properties

The calculated elastic constants for the polymorphs are listed in Table V and compared with the experimental values and other theoretical data.[47,48,49] The number of independent elastic constants is 5 for a hexagonal system or 8 for an orthorhombic system. All calculated results of α- and β-$Mg_2Al_4Si_5O_{18}$ are used to validate the Born–Huang criteria[50] for mechanical stability: a) $c_{44} > 0$, $c_{11} > |c_{12}|$, $(c_{11} + c_{12})\, c_{33} > 2c_{13}^2$ for the hexagonal system; and b) $c_{11} > 0$, $c_{22} > 0$, $c_{33} > 0$, $c_{44} > 0$, $c_{55} > 0$, $c_{66} > 0$, $c_{11} + c_{22} + c_{33} + 2(c_{12} + c_{13} + c_{23}) > 0$, $c_{11} + c_{22} - 2c_{12} > 0$, $c_{11} + c_{33} - 2c_{13} > 0$, $c_{22} + c_{33} - 2c_{23} > 0$ for the orthorhombic system. The results ensure the structural stabilities of the polymorphs under elastic strain perturbations.

Among all elastic constants, c_{11}, c_{22}, and c_{33} represent the stiffness against principal strains, whereas c_{44}, c_{55}, and c_{66} correspond to the resistance to shear deformations. A common feature for both phases is that c_{11}, c_{22}, and c_{33} are much higher than c_{44}, c_{55}, and c_{66}. In addition, the ratios c_{23}/c_{44}, c_{13}/c_{55}, and c_{12}/c_{66} deviating greatly from unity mean the existence of noncentral interatomic forces in the compounds. Moreover, the six main diagonal elements c_{ii} of α-$Mg_2Al_4Si_5O_{18}$ are slightly larger than those of β-$Mg_2Al_4Si_5O_{18}$.

The elastic properties derived from elastic constants are summarized in Table VI, together with experimental values[44,47,48,51,52] for comparison. The polycrystalline bulk modulus B, shear modulus G and Young's modulus E of α-$Mg_2Al_4Si_5O_{18}$ are higher than those of β-$Mg_2Al_4Si_5O_{18}$. The low shear moduli G of cordierite probably originates from the character that tetrahedra at T_1 sites are relatively softer than those at T_2 sites (restrained by the six-member ring in the xy plane along z axis). To evaluate the trend of ductility or brittleness for cordierite, the ratio of B/G is calculated by[53]:

$$\frac{B}{G} = \frac{2(1+\mu)}{3(1-2\mu)} \quad \text{or} \quad \mu = \frac{3B/G - 2}{6B/G + 2} \quad . \qquad (11)$$

In materials with the B/G ratio higher than 1.75, local strain in the region of the fracture extends easily and thus it increases the ductility. On the contrary, decrement of the B/G ratio indicates a higher stress concentration at the root of a crack since plastic flow is relatively difficult. In

TABLE III. Theoretical lattice parameters (a, b, c in Å and α, β, γ in °) of α- and β-$Mg_2Al_4Si_5O_{18}$, together with experimental data for comparison.

Compound	Crystal system	Space group	a	b	c	α	β	γ
α-$Mg_2Al_4Si_5O_{18}$ (Calc.)	Hexagonal	*P6/mcc*	9.663	9.663	9.197	90	90	120
α-$Mg_2Al_4Si_5O_{18}$ (Expt.)[15]			9.768	9.768	9.341	90	90	120
β-$Mg_2Al_4Si_5O_{18}$ (Calc.)	Orthorhombic	*Cccm*	9.721	9.721	9.229	90	90	120.763
β-$Mg_2Al_4Si_5O_{18}$ (Expt.)[15]			9.809	9.809	9.332	90	90	120.648

TABLE IV. Bond lengths (Å) and degree of distortion of polyhedra of α- and β-$Mg_2Al_4Si_5O_{18}$.

Bond	Site	Bond length	Average bond length	Degree of distortion (10^{-4})
$Si_{1/3}Al_{2/3}$–O (α)	T_1	1.680 1.680 1.680 1.680	1.680	0
$Si_{2/3}Al_{1/3}$–O (α)	T_2	1.652 1.652 1.601 1.608	1.628	0.387
Mg–O (α)	M	2.092 2.092 2.092 2.092	2.092	0
	$T_1$6	1.610 1.610 1.610 1.610	1.610	0
Si–O (β)	$T_2$1	1.568 1.587 1.617 1.617	1.597	1.737
	$T_2$3	1.555 1.597 1.618 1.618	1.597	2.585
Al–O (β)	$T_1$1	1.726 1.726 1.727 1.727	1.727	0.0003
	$T_2$6	1.681 1.684 1.744 1.744	1.714	3.204
Mg–O (β)	M	2.086 2.086 2.095 2.095 2.095 2.095	2.092	0.0197

https://doi.org/10.1557/jmr.2015.367 Published online by Cambridge University Press

the present case, the *B/G* ratios for α- and β-$Mg_2Al_4Si_5O_{18}$ are 2.44 and 2.49, respectively. It means that both phases are possibly quasi-ductile and that Al/Si-disordered α phase is a little more brittle than the ordered β phase.

The α- and β-$Mg_2Al_4Si_5O_{18}$ with hexagonal and orthorhombic crystal systems are expected anisotropic elasticity. We herein use the classical Zener[54] index to measure the degree of elastic anisotropy. Three shear anisotropic parameters A_1, A_2, A_3 or namely Zener ratios are calculated for the (100), (010), and (001) shear planes:

$$A_1 = 4c_{44}/(c_{22} + c_{33} - 2c_{23})$$
$$A_2 = 4c_{55}/(c_{11} + c_{33} - 2c_{13}) \quad (12)$$
$$A_3 = 4c_{66}/(c_{11} + c_{22} - 2c_{12}) \quad .$$

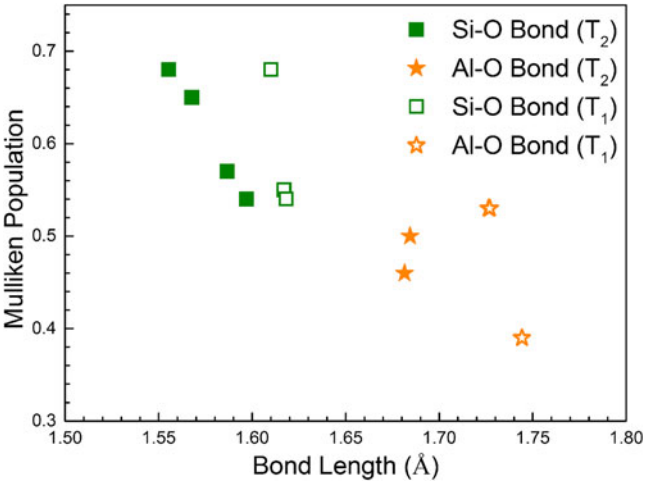


FIG. 2. Mulliken Populations of Si–O and Al–O bonds in β-$Mg_2Al_4Si_5O_{18}$.

For a material with elastic anisotropy, all Zener ratios would obviously deviate from unity. As shown in Table VII, both phases have nonunity Zener ratios and the results demonstrate anisotropic elastic stiffness.

Consequently, directional Young's moduli[35] of α- and β-$Mg_2Al_4Si_5O_{18}$ are calculated by the equation expressed in the Einstein summation convention:

$$E_n = 1/n_i n_j S_{ijkl} n_k n_l \quad (i,j,k,l = 1,2,3) \quad , \quad (13)$$

Here, n_i, n_j, n_k, and n_l are the direction cosines of angles with the three principal directions and S_{ijkl} is the elastic compliance (inverse of stiffness tensor).

Figure 3 and Fig. 4 show the directional Young's moduli of both phases by the color map as well as three projections along the *x*, *y*, *z* axes. Directional dependences of Young's Modulus for α- and β-$Mg_2Al_4Si_5O_{18}$ display weak anisotropy. Hexagonal α-$Mg_2Al_4Si_5O_{18}$ are elastically isotropic in the *xy* plane, which means that the elastic constants are invariant to arbitrary rotations around the *z* axis [see Fig. 3(d)]. This condition is called transverse isotropy.[55] The root of this consequence is the symmetry restriction ($c_{66} = (c_{11} - c_{12})/2$) in hexagonal crystals. In the meantime, orthorhombic β-$Mg_2Al_4Si_5O_{18}$ without the restriction is anisotropic in the xy plane [see Fig. 4(d)]. Young's modulus of β-$Mg_2Al_4Si_5O_{18}$ is 154.5 GPa along the *x* axis and 145.7 along the *y* axis. The maximum value of the Young's modulus is 165.6 GPa along all directions in the *xy* plane for α-$Mg_2Al_4Si_5O_{18}$ and 154.5 GPa along the x axis for β-$Mg_2Al_4Si_5O_{18}$. The minimum values of Young's modulus for α- and β-$Mg_2Al_4Si_5O_{18}$ are 137.2 and 128.6 GPa, respectively, along the *z* axis.

TABLE V. Theoretical elastic constants (GPa) of α- and β-$Mg_2Al_4Si_5O_{18}$ together with experimental data and another calculation for comparison.

Compound	c_{11}	c_{22}	c_{33}	c_{44}	c_{55}	c_{66}	c_{12}	c_{23}	c_{13}
α-$Mg_2Al_4Si_5O_{18}$ (Calc.)	232	232	200	54	54	65	103	103	103
α-$Mg_2Al_4Si_5O_{18}$ (Expt.[47])	201	201	176	47	47	58	86	84	84
β-$Mg_2Al_4Si_5O_{18}$ (Calc.)	220	214	190	54	48	64	102	97	100
β-$Mg_2Al_4Si_5O_{18}$ (Expt.[48])	207	214	186	47	52	64	94	89	95
β-$Mg_2Al_4Si_5O_{18}$ (Calc.[49])	209	202	195	51	46	64	94	85	84

TABLE VI. Theoretical polycrystalline bulk modulus *B* (GPa), shear modulus *G* (Gpa), Pugh's ratio *G/B*, Young's modulus *E* (GPa) and Poisson's ratio ν.

Compound	B	G	B/G	E	ν
α-$Mg_2Al_4Si_5O_{18}$ (Calc.)	142	58	2.444	154	0.320
α-$Mg_2Al_4Si_5O_{18}$ (Expt.)	...	47.3 (Ref. 47)	...	139 (Ref. 51), 164 (Ref. 51), 148 (Ref. 47)	0.28 (Ref. 47), 0.34 (Ref. 47)
β-$Mg_2Al_4Si_5O_{18}$ (Calc.)	136	55	2.490	144	0.323
β-$Mg_2Al_4Si_5O_{18}$ (Expt.)	129 (Ref. 48), 119 (Ref. 52), 131 (Ref. 44)	54 (Ref. 48)	...	...	...

https://doi.org/10.1557/jmr.2015.367 Published online by Cambridge University Press

TABLE VII. The shear anisotropy factors or Zener ratios of α- and β-$Mg_2Al_4Si_5O_{18}$ obtained from theoretical calculation.

Compound	A_1	A_2	A_3
α-$Mg_2Al_4Si_5O_{18}$ (Calc.)	0.958	0.958	0.840
β-$Mg_2Al_4Si_5O_{18}$ (Calc.)	1.068	0.880	1.118

C. Thermal conductivity

Lattice thermal conductivity is determined by various phonon scattering mechanisms, from boundary scattering to phonon–phonon Umklapp scattering with increasing temperature.[56,57] Slack[24] proposed the widely accepted model, i.e., Eq. (4), to depict the lattice thermal conductivity at a moderately high temperature. In such a case, the predominant scattering mechanism is the intrinsic phonon–phonon Umklapp scattering and the heat is transported primarily by acoustic phonons.

Table VIII presents the parameters used for the calculation of thermal conductivity from Slack and Clarke models [see Eqs. (4) and (10)]. As mentioned above, the sound velocities v_l, v_s, v_m and Debye temperature θ_D are estimated from elastic constants [see Eqs. (7)–(9)]. Also, the Grüneisen parameter γ is obtained from Poisson's ratio ν [see Eq. (6)]. Figure 5 shows the temperature-dependent thermal conductivities predicted by the Slack model for both phases, together with some complex ceramics with low thermal conductivity.[4,58,59] The thermal conductivity at RT is very low, 2.95 and 2.64 W/(m·K) for α- and β-$Mg_2Al_4Si_5O_{18}$. As the temperature increases, thermal conductivity decreases with reciprocal T as described by Eq. (4). Thermal conductivity approaches its minimum value estimated by the Clarke model [see Eq. (10)], about 1.33 W/(m·K) for α-$Mg_2Al_4Si_5O_{18}$ at 605 K and 1.29 W/(m·K) for β-$Mg_2Al_4Si_5O_{18}$ at 558 K. As discussed above, the VCA method increases the symmetry and decreases the freedom of α-$Mg_2Al_4Si_5O_{18}$ compared to its real local structure. So the predicted thermal conductivity of α-$Mg_2Al_4Si_5O_{18}$ would be slightly overestimated. It is also expect that the actual value will to be very close to that of β-$Mg_2Al_4Si_5O_{18}$. Generally, the polymorphs have quite similar physical and chemical properties so they are not normally distinguished in the ceramic society. As the temperature increases further, thermal conductivity will no longer decrease because phonon mean free path reaches its lower bound limited by the average atomic distance δ. In other words, theoretical lattice thermal conductivity below the calculated minimum value is of no practical concern. From room to high temperature, the thermal conductivity of cordierite shows low magnitude and just changes within a narrow range, 2.9–1.3 W/(m·K), which is preferred in applications as thermal insulators.

To better understand the physical origin of the very low thermal conductivity of $Mg_2Al_4Si_5O_{18}$, Lu_2SiO_5[59] reference material with the lowest thermal conductivity in Fig. 5 is selected as a comparison because: (i) Its crystal structure consists of similar polyhedral framework to $Mg_2Al_4Si_5O_{18}$ except that $Mg_2Al_4Si_5O_{18}$ contains loosely bound Mg atoms; (ii) Both of Lu_2SiO_5 and $Mg_2Al_4Si_5O_{18}$ are silicates, but the former contains heavy

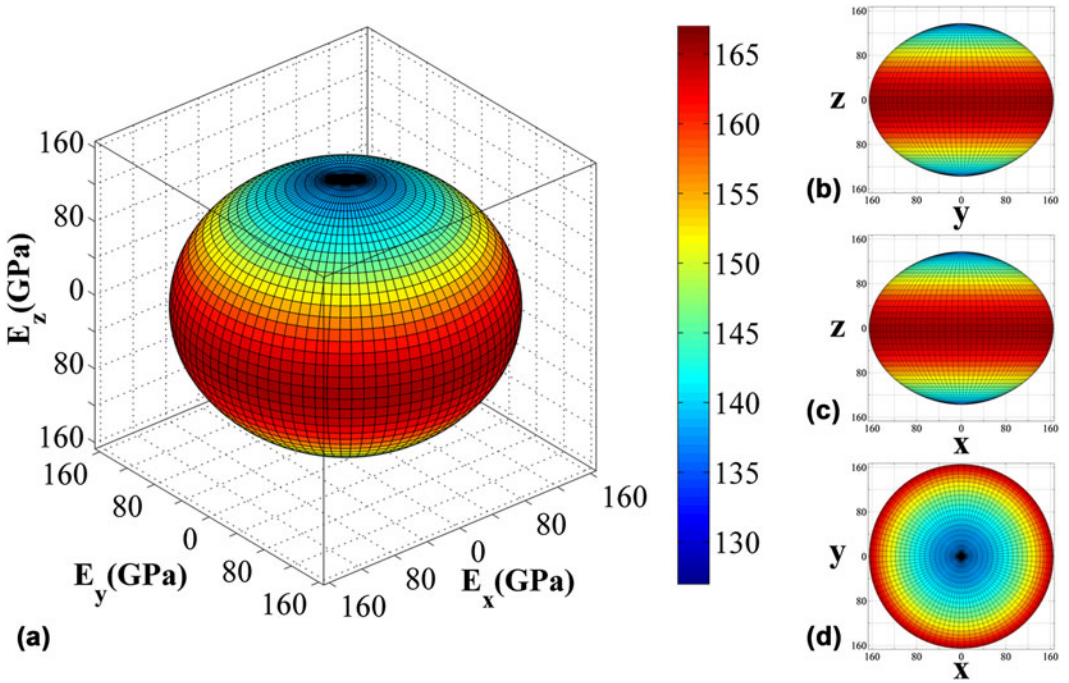


FIG. 3. (a) Direction-dependent Young's modulus of α-$Mg_2Al_4Si_5O_{18}$ and its projection along (b) x, (c) y, and (d) z axes.

https://doi.org/10.1557/jmr.2015.367 Published online by Cambridge University Press

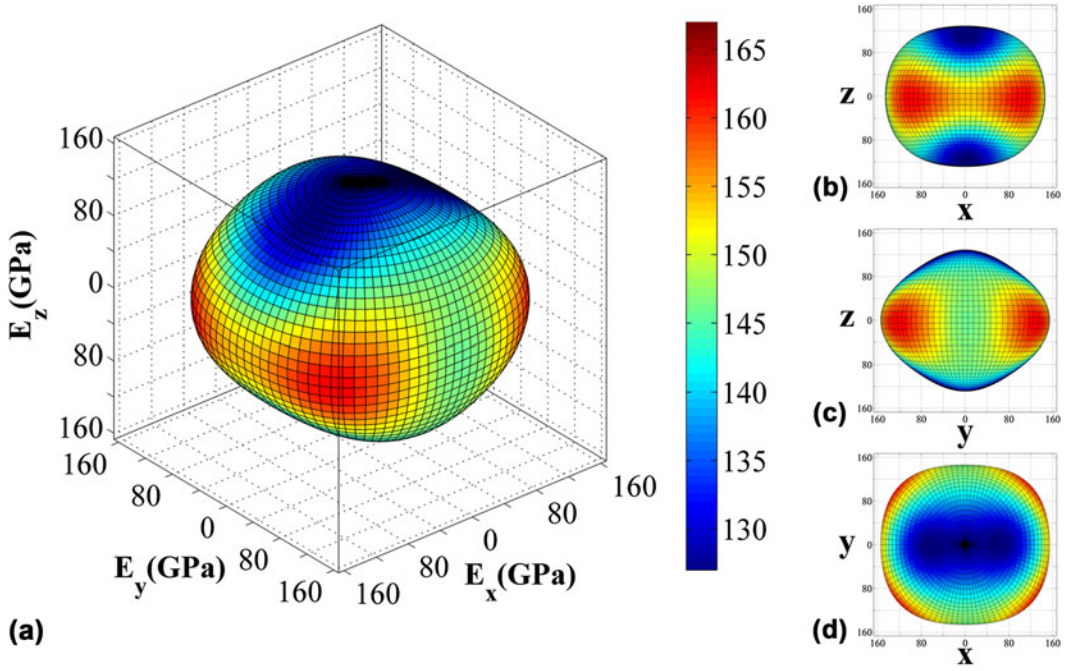


FIG. 4. (a) Direction-dependent Young's modulus of β-$Mg_2Al_4Si_5O_{18}$ and its projection along (b) *x*, (c) *y* and (d) *z* axes.

TABLE VIII. Theoretical values of average atomic mass $\bar{M}$ (g/mol), average distance between atoms δ (Å), number of atoms per primitive unit cell N_{cell}, density ρ (g/cm^3), sound velocities (v_l, v_s, v_m in km/s), Debye temperature θ_D (K), Grüneisen parameter γ, and minimum thermal conductivity κ_{min} [W/(m·K)] for polycrystalline cordierite polymorphs, together with Lu_2SiO_5 for comparison.

Compound	$\bar{M}$	δ	N_{cell}	ρ	v_l	v_t	v_m	θ_D	γ	κ_{min}	$\kappa \cdot T$
α-$Mg_2Al_4Si_5O_{18}$ (Calc.)	20.16	2.34	58	2.61	4.72	9.17	5.29	673	1.90	1.33	805
β-$Mg_2Al_4Si_5O_{18}$ (Calc.)	20.16	2.35	58	2.59	4.59	8.97	5.14	652	1.92	1.29	720
Lu_2SiO_5 (Calc.)	57.25	2.34	32	7.38	5.214	3.002	3.334	423	1.5	0.84	1359

Lutetium atoms while the latter is free of the rare-earth element. These are representative materials for weighting the possible strategies to develop a novel candidate with very low thermal conductivity.

As a well-established method for evaluating thermal conductivity among numerous materials, the Slack model by itself provides important information for material selection. Equation (4) can be mathematically factorized into three parts, the number of atoms per cell N_{cell}, Grüneisen parameter γ, and Debye temperature θ_D, by which thermal conductivity of a material is determined. The power values of N_{cell}, γ and θ_D are −2/3, −2, and 3, respectively, in Eq. (4), so that a tiny increment of γ or N_{cell} or decrement of θ_D would obviously decrease thermal conductivity. $Mg_2Al_4Si_5O_{18}$ has a higher Debye temperature θ_D (652 K) than Lu_2SiO_5 (423 K) but it still holds lower thermal conductivity (2.64 W/(m·K) for β-$Mg_2Al_4Si_5O_{18}$) than Lu_2SiO_5 [4.98 W/(m·K)] at RT. Therefore, θ_D is not the determinant factor of the low thermal conductivity of $Mg_2Al_4Si_5O_{18}$. In addition, they both have nearly the same atomic distance, δ = 2.35 Å, in the sparse crystal structures. Parameter δ is also screened out the key factor for the divergence of thermal conductivity.

The other two parameters, the Grüneisen parameter γ and number of atoms per cell N_{cell} of $Mg_2Al_4Si_5O_{18}$, are the predominant reasons for its low lattice thermal conductivity. The Grüneisen parameter of $Mg_2Al_4Si_5O_{18}$ is about 30% higher than Lu_2SiO_5 (1.92 for $Mg_2Al_4Si_5O_{18}$ and 1.5 for Lu_2SiO_5), which may lead to more than 40% decrease in the magnitude of thermal conductivity. The larger γ indicates a higher level of anharmonic phonon scattering in $Mg_2Al_4Si_5O_{18}$, which is the origin of higher thermal resistance. The huge anharmonicity relates to the significant distortions of polyhedra and strong noncentral interatomic forces in $Mg_2Al_4Si_5O_{18}$, as well as the loosely bound Mg atoms within the AlO_4 or SiO_4 tetrahedra framework.

Furthermore, it is worthy of discussing the physical scheme on how the number of atoms in the primitive cell, N_{cell}, affects the lattice thermal conductivity of $Mg_2Al_4Si_5O_{18}$. It qualitatively characterizes the effects of structural complexity on lattice thermal conductivity. The N_{cell} is 58 for $Mg_2Al_4Si_5O_{18}$ (in contrast, only 32 atoms for

https://doi.org/10.1557/jmr.2015.367 Published online by Cambridge University Press

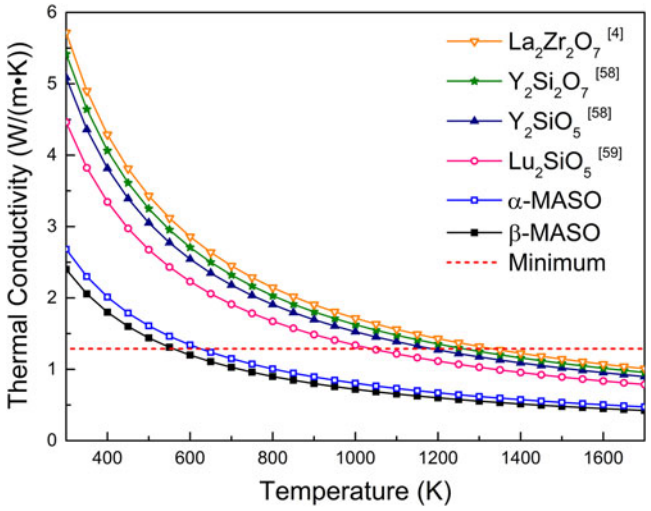


FIG. 5. Temperature dependences of thermal conductivities of α- and β-$Mg_2Al_4Si_5O_{18}$, together with other complex ceramics for comparison. The theoretical minimum thermal conductivity is also shown as dashed line.

Lu_2SiO_5). As the N_{cell} increases, the lattice parameters increase in real space and the position of the Brillouin zone boundary in reciprocal space moves inward and cuts the acoustic phonon branch with lower frequency. Simultaneously, the phonon dispersion "folds in" on itself as the N_{cell} increases.[60,61] These two physical mechanisms will decrease the group velocity v of acoustic phonons as well as the acoustic Debye temperature[61,62] (defined as $\theta_a = \theta_D/N_{cell}^{1/3}$). Hence the lattice thermal conductivity is significantly decreased by increasing the number of atoms in the primitive cell.

The last discussion is addressed to the character of low density, or lightweight of $Mg_2Al_4Si_5O_{18}$. $Mg_2Al_4Si_5O_{18}$ has smaller average mass of atoms or lower density than Lu_2SiO_5, namely the density is only 1/3 of the value of Lu_2SiO_5. However, the lattice thermal conductivity of $Mg_2Al_4Si_5O_{18}$ yields a much lower value compared with its competitor Lu_2SiO_5 with a heavy rare-earth element. This result provides exciting information that it is possible to achieve very low thermal conductivity in lightweight materials. This is in contrast to our general knowledge on increasing the average atomic mass or incorporating rare-earth element to effectively block heat transportation.[63–65] We herein highlight a perspective on developing a promising candidate with low thermal conductivity through tailoring the complexity of the crystal structure. To summarize, the lattice thermal conductivity is predominantly determined by Debye temperature, Grüneisen parameter, the number of atoms per primitive unit cell, as well as the mean atomic mass. To select an alternative strategy, giant anharmonicity of phonon scattering, giant structural complexity, and low density are believed to bring out the extremely low thermal conductivity in some lightweight materials like $Mg_2Al_4Si_5O_{18}$.

IV. CONCLUSION

Equilibrium structures, bonding characteristics, mechanical properties, and thermal conductivities of two cordierite polymorphs, α-$Mg_2Al_4Si_5O_{18}$ and β-$Mg_2Al_4Si_5O_{18}$, are predicted by first-principle total energy calculations. VCA method is verified by comparison between theoretical and experimental results. Crystal structure and chemical bonding analysis indicate that isolated Mg atoms are loosely bound with surrounding framework of Al/Si tetrahedra, generally resulting in the decrease of thermal conductivity. Elastic constants, polycrystalline moduli, Poisson's ratio, elastic anisotropy, and directional Young's modulus are discussed with respect to the crystal structure. Generally speaking, α-$Mg_2Al_4Si_5O_{18}$ has slightly higher mechanical properties than β-$Mg_2Al_4Si_5O_{18}$. Sound velocities, Debye temperature, and Grüneisen parameter are derived from the above parameters and are used to predict the temperature-dependent lattice thermal conductivity of cordierite and its minimum value by Slack's and Clarke's models. The intrinsic lattice thermal conductivities of α- and β-$Mg_2Al_4Si_5O_{18}$ decrease with temperature as $804.6/T$ and $719.7/T$, respectively, and then approach the theoretical minimum values at high temperatures. The present results and related discussions suggest that the unique complex crystal structure of cordierite plays a key role in decreasing the thermal conductivity. Finally it is addressed that $Mg_2Al_4Si_5O_{18}$ is a promising lightweight ceramic with extremely low thermal conductivity.

ACKNOWLEDGMENTS

This work was supported by the Natural Sciences Foundation of China under Grant Nos. 51032006 and 51372252.

REFERENCES

1. D.R. Clarke: Materials selection guidelines for low thermal conductivity thermal barrier coatings. *Surf. Coat. Technol.* **163–164**, 67 (2003).
2. L. Sun, B. Liu, J. Wang, J. Wang, Y. Zhou, and Z. Hu: $Y_4Si_2O_7N_2$: A new oxynitride with low thermal conductivity. *J. Am. Ceram. Soc.* **95**(10), 3278 (2012).
3. B. Liu, J.Y. Wang, Y.C. Zhou, T. Liao, and F.Z. Li: Theoretical elastic stiffness, structure stability and thermal conductivity of $La_2Zr_2O_7$ pyrochlore. *Acta Mater.* **55**(9), 2949 (2007).
4. J. Feng, B. Xiao, R. Zhou, and W. Pan: Thermal conductivity of rare earth zirconate pyrochlore from first principles. *Scr. Mater.* **68**(9), 727 (2013).
5. Y. Zhou and B. Liu: Theoretical investigation of mechanical and thermal properties of MPO_4 (M=Al, Ga). *J. Eur. Ceram. Soc.* **33**(13–14), 2817 (2013).
6. A. Du, C. Wan, Z. Qu, and W. Pan: Thermal conductivity of Monazite-type $REPO_4$ (RE=La, Ce, Nd, Sm, Eu, Gd). *J. Am. Ceram. Soc.* **92**(11), 2687 (2009).
7. W.D. Kingery, H.K. Bowen, and D.R. Unhlmann: *Introduction to ceramics* (2nd ed.) (New York: John Wiley & Sons, Inc., 1976).
8. X. Cao, R. Vassen, and D. Stoever: Ceramic materials for thermal barrier coatings. *J. Eur. Ceram. Soc.* **24**(1), 1 (2004).

https://doi.org/10.1557/jmr.2015.367 Published online by Cambridge University Press

9. Z. Sun, M. Li, and Y. Zhou: Thermal properties of single-phase Y_2SiO_5. *J. Eur. Ceram. Soc.* **29**(4), 551 (2009).
10. Z. Sun, Y. Zhou, J. Wang, and M. Li: Thermal properties and thermal shock resistance of γ-$Y_2Si_2O_7$. *J. Am. Ceram. Soc.* **91**(8), 2623 (2008).
11. H. Xiang, Z. Feng, and Y. Zhou: Dynamical and dielectric properties of MP_2O_7 (M = Ti, Zr, and Hf): A first-principles investigation. *Comput. Mater. Sci.* **95**, 371 (2014).
12. H. Xiang, Z. Feng, and Y. Zhou: Ab initio computations of electronic, mechanical, lattice dynamical and thermal properties of ZrP_2O_7. *J. Eur. Ceram. Soc.* **34**(7), 1809 (2014).
13. H. Xiang, Z. Feng, Z. Li, and Y. Zhou: Theoretical investigations on mechanical and thermal properties of $MSiO_4$ (M = Zr, Hf). *J. Mater. Res.* **30**(13), 2030 (2015).
14. J. Fulmer, O.I. Lebedev, V.V. Roddatis, D.C. Kaseman, S. Sen, J-A. Dolyniuk, K. Lee, A.V. Olenev, and K. Kovnir: Clathrate $Ba_8Au_{16}P_{30}$: The "gold standard" for lattice thermal conductivity. *J. Am. Chem. Soc.* **135**(33), 12313 (2013).
15. B. Winkler, M.T. Dove, and M. Leslie: Static lattice energy minimization and lattice dynamics calculations on aluminosilicate minerals. *Am. Mineral.* **76**, 313 (1991).
16. P.W. Mirwald: Thermal expansion of anhydrous Mg-cordierite between 25 and 950° C. *Phys. Chem. Miner.* **7**(6), 268 (1981).
17. H. Ohsato, J-S. Kim, C-I. Cheon, and I. Kagomiya: Millimeter-wave dielectrics of indialite/cordierite glass ceramics: Estimating Si/Al ordering by volume and covalency of Si/Al octahedron. *J. Ceram. Soc. Jpn.* **121**(1416), 649 (2013).
18. A. Yamuna, S. Honda, K. Sumita, M. Yanagihara, S. Hashimoto, and H. Awaji: Synthesis, sintering and thermal shock resistance estimation of porous cordierite by IR heating technique. *Microporous Mesoporous Mater.* **85**(1–2), 169 (2005).
19. M.A. Camerucci, G. Urretavizcaya, M.S. Castro, and A.L. Cavalieri: Electrical properties and thermal expansion of cordierite and cordierite-mullite materials. *J. Eur. Ceram. Soc.* **21**(16), 2917 (2001).
20. M.E. Milberg and H.D. Blair: Thermal expansion of cordierite. *J. Am. Ceram. Soc.* **60**(7–8), 372 (1977).
21. D.L. Evans, G.R. Fischer, J.E. Geiger, and F.W. Martin: Thermal expansions and chemical modifications of cordierite. *J. Am. Ceram. Soc.* **63**(11–12), 629 (1980).
22. Q. Liu, Z. Liu, and Z. Huang: CuO supported on Al_2O_3-coated cordierite-honeycomb for SO_2 and no removal from flue gas: Effect of acid treatment of the cordierite. *Ind. Eng. Chem. Res.* **44**(10), 3497 (2005).
23. Y. Dong, X. Feng, D. Dong, S. Wang, J. Yang, J. Gao, X. Liu, and G. Meng: Elaboration and chemical corrosion resistance of tubular macro-porous cordierite ceramic membrane supports. *J. Membr. Sci.* **304**(1–2), 65 (2007).
24. G.A. Slack: The thermal conductivity of nonmetallic crystals. *Solid State Phys.* **34**, 1 (1979).
25. D.M. Ceperley and B.J. Alder: Ground state of the electron gas by a stochastic method. *Phys. Rev. Lett.* **45**(7), 566 (1980).
26. M.D. Segall, J.D.L. Philip, M.J. Probert, C.J. Pickard, P.J. Hasnip, S.J. Clark, and M.C. Payne: First-principles simulation: Ideas, illustrations and the CASTEP code. *J. Phys.: Condens. Matter* **14**(11), 2717 (2002).
27. D. Vanderbilt: Soft self-consistent pseudopotentials in a generalized eigenvalue formalism. *Phys. Rev. B* **41**(11), 7892 (1990).
28. H.J. Monkhorst and J.D. Pack: Special points for Brillouin-zone integrations. *Phys. Rev. B* **13**(12), 5188 (1976).
29. B.G. Pfrommer, M. Côté, S.G. Louie, and M.L. Cohen: Relaxation of crystals with the quasi-Newton method. *J. Comput. Phys.* **131**(1), 233 (1997).
30. L. Bellaiche and D. Vanderbilt: Virtual crystal approximation revisited: Application to dielectric and piezoelectric properties of perovskites. *Phys. Rev. B* **61**(12), 7877 (2000).
31. B. Winkler, C. Pickard, and V. Milman: Applicability of a quantum mechanical 'virtual crystal approximation' to study Al/Si-disorder. *Chem. Phys. Lett.* **362**(3–4), 266 (2002).
32. V. Milman and M.C. Warren: Elasticity of hexagonal BeO. *J. Phys.: Condens. Matter* **13**(2), 241 (2001).
33. E. Makovicky and T. Balic-Zunic: New measure of distortion for coordination polyhedra. *Acta Crystallogr., Sect. B* **54**(6), 766 (1998).
34. R. Hill: The elastic behaviour of a crystalline aggregate. *Proc. Phys. Soc., London, Sect. A* **65**(5), 349 (1952).
35. J.F. Nye: *Physical Properties of Crystals* (New York: Oxford University Press, 1985).
36. D. Morelli, V. Jovovic, and J. Heremans: Intrinsically minimal thermal conductivity in cubic I-V-VI_2 semiconductors. *Phys. Rev. Lett.* **101**(3), 035901 (2008).
37. J.W. Zwanziger: Phonon dispersion and Grüneisen parameters of zinc dicyanide and cadmium dicyanide from first principles: Origin of negative thermal expansion. *Phys. Rev. B* **76**(5), 052102 (2007).
38. D.S. Sanditov, V.V. Mantatov, M.V. Darmaev, and B.D. Sanditov: On the Gruneisen parameter for crystals and glasses. *Tech. Phys.* **54**(3), 385 (2009).
39. O.L. Anderson: The debye temperature of vitreous silica. *J. Phys. Chem. Solids* **12**(1), 41 (1959).
40. B. Liu, J.Y. Wang, F.Z. Li, and Y.C. Zhou: Theoretical elastic stiffness, structural stability and thermal conductivity of $La_2T_2O_7$ (T=Ge, Ti, Sn, Zr, Hf) pyrochlore. *Acta Mater.* **58**(13), 4369 (2010).
41. K. Leont'ev: O vzaimosvyazi mezhdu uprugimi i teplovymi svoistvami tverdykh tel. *Akust. Zh.* **47**(4), 554 (1981).
42. J.P. Cohen, F.K. Ross, and G.V. Gibbs: An X-ray and neutron diffraction study of hydrous low cordierite. *Am. Mineral.* **62**(1–2), 67 (1977).
43. E.P. Meagher and G.V. Gibbs: The polymorphism of cordierite; II, the crystal structure of indialite. *Can. Mineral.* **15**(1), 43 (1977).
44. R. Miletich, G.D. Gatta, T. Willi, P.W. Mirwald, P. Lotti, M. Merlini, N. Rotiroti, and T. Loerting: Cordierite under hydrostatic compression: Anomalous elastic behavior as a precursor for a pressure-induced phase transition. *Am. Mineral.* **99**(2–3), 479 (2014).
45. P.W. Mirwald, M. Malinowski, and H. Schulz: Isothermal compression of low-cordierite to 30 kbar (25° C). *Phys. Chem. Miner.* **11**(3), 140 (1984).
46. R.S. Mulliken: Electronic population analysis on LCAO–MO molecular wave functions. II. Overlap populations, bond orders, and covalent bond energies. *J. Chem. Phys.* **23**(10), 1841 (1955).
47. C. Bubeck: Direction dependent mechanical properties of extruded cordierite honeycombs. *J. Eur. Ceram. Soc.* **29**(15), 3113 (2009).
48. K. Toohill, S. Siegesmund, and J.D. Bass: Sound velocities and elasticity of cordierite and implications for deep crustal seismic anisotropy. *Phys. Chem. Miner.* **26**(4), 333 (1999).
49. V.L. Vinograd, L.L. Perchuk, T.V. Gerya, A. Putnis, B. Winkler, and J.D. Gale:Order/disorder phase transition in cordierite and its possible relationship to the development of symplectite reaction textures in granulites. *Petrology* **15**(5), 427 (2007).
50. M. Born and K. Huang: *Dynamical theory of crystal lattices* (Oxford: Oxford University Press, 1998).
51. T. Ogiwara, Y. Noda, K. Shoji, and O. Kimura: Low temperature sintering of alpha-cordierite ceramics with low thermal expansion using Li_2O-Bi_2O_3 as a sintering additive. *J. Ceram. Soc. Jpn.* **119**(1393), 706 (2011).
52. J. Koepke and H. Schulz: Single crystal structure investigations under high-pressure of the mineral cordierite with an improved high-pressure cell. *Phys. Chem. Miner.* **13**(3), 165 (1986).
53. S.F. Pugh: XCII. Relations between the elastic moduli and the plastic properties of polycrystalline pure metals. *London, Edinburgh Dublin Philos. Mag. J. Sci.* **45**(367), 823 (1954).

https://doi.org/10.1557/jmr.2015.367 Published online by Cambridge University Press

54. C. Zener: *Elasticity and Anelasticity of Metals* (Chicago: University of Chicago Press, 1948).
55. H.M. Ledbetter: Elastic properties of zinc: A compilation and a review. *J. Phys. Chem. Ref. Data* **6**(4), 1181 (1977).
56. T.M. Tritt: *Thermal Conductivity: Theory, Properties, and Applications* (New York: Kluwer Academic/Plenum Publishers, 2004).
57. E.S. Toberer, L.L. Baranowski, and C. Dames: Advances in thermal conductivity. *Annu. Rev. Mater. Res.* **42**(1), 179 (2012).
58. Y. Luo, J. Wang, J. Wang, J. Li, and Z. Hu: Theoretical predictions on elastic stiffness and intrinsic thermal conductivities of yttrium silicates. *J. Am. Ceram. Soc.* **97**(3), 945 (2014).
59. Z. Tian, L. Sun, J. Wang, and J. Wang: Theoretical prediction and experimental determination of the low lattice thermal conductivity of Lu_2SiO_5. *J. Eur. Ceram. Soc.* **35**(6), 1923 (2015).
60. Y. Luo, J. Wang, J. Li, Z. Hu, and J. Wang: Theoretical study on crystal structures, elastic stiffness, and intrinsic thermal conductivities of β-, γ-, and δ-$Y_2Si_2O_7$. *J. Mater. Res.* **30**(04), 493 (2015).
61. E.S. Toberer, A. Zevalkink, and G.J. Snyder: Phonon engineering through crystal chemistry. *J. Mater. Chem.* **21**(40), 15843 (2011).
62. M. Roufosse and P.G. Klemens: Thermal conductivity of complex dielectric crystals. *Phys. Rev. B* **7**(12), 5379 (1973).
63. J. Feng, B. Xiao, R. Zhou, and W. Pan: Thermal expansion and conductivity of $RE_2Sn_2O_7$ (RE=La, Nd, Sm, Gd, Er and Yb) pyrochlores. *Scr. Mater.* **69**(5), 401 (2013).
64. Z-G. Liu, J-H. Ouyang, Y. Zhou, and X-L. Xia: Electrical conductivity and thermal expansion of neodymium–ytterbium zirconate ceramics. *J. Power Sources* **195**(10), 3261 (2010).
65. Q. Xu, W. Pan, J. Wang, C. Wan, L. Qi, H. Miao, K. Mori, and T. Torigoe: Rare-earth zirconate ceramics with fluorite structure for thermal barrier coatings. *J. Am. Ceram. Soc.* **89**(1), 340 (2006).

https://doi.org/10.1557/jmr.2015.367 Published online by Cambridge University Press